N O T I C E

BER

GRAPHITE FORMATION IN CAST IRON
(PHASE II)

Final Report

by

Dr. Doru M. Stefanescu, Professor
Department of Metallurgical Engineering
College of Engineering
The University of Alabama

and

Michael R. Fiske
Graduate Research Assistant

Prepared for

June 1985

BER REPORT NO. 354-202

GRAPHITE FORMATION IN CAST IRON (PHASE II)

Final Report

by

Dr. Doru M. Stefanescu, Professor
Department of Metallurgical Engineering
College of Engineering
The University of Alabama

and

Michael R. Fiske
Graduate Research Assistant

Prepared for

June 1985

BER Report No. 354-202

1. INTRODUCTION

Between the summer of 1984 and spring of 1985, several types of cast irons were directionally solidified aboard the KC-135 aircraft. Also, control samples were run on Earth for comparison. Some of these samples were unusable because of various mechanical problems, and this report covers the analysis and the interpretation of results on the samples that were run successfully.

2. EQUIPMENT

All samples were solidified in a Bridgeman-type Automatic Directional Solidification Furnace (A.D.S.F.) which has been described previously (1).

3. SAMPLE PREPARATION

All samples were prepared from laboratory grade materials. These included 99%+ pure iron powder, 99.99%+ pure graphite powder, and 99.9%+ pure Si. Chunk Ce or industrial grade Fe_3P was added as desired. The base materials (Fe, C, Si) were melted as 250 gm heats in alumina crucibles in a Jelrus Super-Melt electric resistance furnace, superheated to 1450°C, Ce or Fe_3P added and held for 5 minutes, and then poured into a preheated steel mold to produce rods approximately 127 mm long with diameters of 4 and/or 10 mm.

4. EXPERIMENTAL CONDITIONS

The analysis of the samples run and analyzed/interpreted are as

follows:

Series No.	Chemical Analysis %						Carbon Equivalent
	C	Si	Mn	P	S	Ce	
P-2	4.08	2.39	.020	.007	.011	.001	4.88
84-F-4	3.61	1.80	.033	.10	.001	.001	4.24
84-F-11	4.33	1.53	.052	.10	.011	.001	4.87
84-F-6	3.68	2.57	.40	.25	.002	.001	4.62
84-F-3	4.28	0.01	.016	.003	.002	.001	4.28
84-F-9	4.41	1.68	.050	.007	.009	.001	4.97
84-F-8	3.88	2.18	.040	.005	.006	> .07	4.61

The samples were directionally solidified in a Bridgeman type

furnace under the following experimental conditions:

Sample No.	Date Flown	Translation Rate mm/min	Temperature Gradient °C/cm	Control Temp. °C
KC-135 A.D.S.F. Flight Samples				
P-2	6-20-84	5.16	330	1320
P-2	8-21-84	2.00	330	1320
84-F-4	12-17-84	0.80	330	1305
84-F-4	12-19-84	2.05	330	1318
84-F-11	12-18-84	2.02	330	1320
84-F-6	12-18-84	4.08	330	1320
84-F-6	7-17-84	4.85	330	1305
84-F-3	6-20-84	5.17	201	1195
84-F-9	7-17-84	4.89	201	1190
84-F-8	7-17-84	4.97	201	1190
A.D.S.F. Control Samples				
P-2	12-4-84	4.79	330	1320
84-F-6	12-4-84	5.06	330	1305
84-F-3	12-4-84	4.69	201	1195
84-F-9	12-4-84	5.17	201	1190
84-F-8	12-4-84	5.19	201	1190

5. RESULTS

5.1 Sample P-2 (pure Fe-C-Si alloy), R=5.16 mm/min.

A composite metallographic picture of this sample is shown in Figure 1. Solidification started without a run-up in the first low-g parabola. It can be seen that the structure in the first low-g zone consists of fine irregular graphite embedded in a pearlitic matrix. This is also shown on Figure 2a. As soon as the first high-g zone starts, some typical flake graphite solidifies alternating with coarse graphite (Figures 1 and 2b). At about the middle of the first high-g zone a highly oriented band of flake graphite can be observed, as shown on both Figure 1 at low magnification, and on Figure 2c at higher magnification.

This band is then followed by a zone similar in structure with the first low-g zone with the exception that the irregular graphite is slightly coarser (Figure 2d). No significant change in structure was apparent at the transition from the first high-g zone to the second low-g zone. Nevertheless, the irregular graphite becomes even coarser toward the end of the second low-g zone and the beginning of the second high-g zone, and then again at the transition from the third low-g zone to the third high-g zone. Another significant structural change along the sample is related to the austenite dendrites. Although the iron is of strongly hypereutectic composition, austenite dendrites can be observed over most of the length of the sample, with the exception of the first half of the first high-g zone. The degree of orientation in the direction of the heat flow increases along the sample, and the dendrites become longer.

High segregation supposedly occurring toward the end of the sample results in a complex structure as shown in Figure 1.

5.2 Sample P-2 (pure Fe-C-Si alloy) R=2.00 mm/min.

The sample exhibits fine graphite flakes, with small dendrites beginning to grow in the third low-g zone. At the beginning of the fourth high-g zone, dendrites are much larger, and primary graphite formations begin appearing, especially at the walls. The rest of the sample is marked by primary graphite nucleating at the walls on both sides of the sample.

In the seventh low-g zone, primary graphite formations become much larger, and the transition from the seventh high-g to eighth low-g zones is marked by a band of very large primary graphite formations. The eighth low-g zone is the last that is specified by accelerometer data, but the rest of the sample shows an increase in primary graphite formations.

5.3 Sample 84-F-4 (pure Fe-C-Si-P alloy), R=0.8 mm/min.

The interface is clearly marked by a band of highly oriented eutectic graphite surrounded by very fine pearlite. This band extends through the first low-g zone to the center of the first high-g zone.

From here to the beginning of the second high-g zone, pearlite and ferrite are present. At the beginning of the second high-g zone however, large eutectic cells begin forming and are present to the end of the sample. They appear to be equiaxed, except that there appears to be a higher concentration of flake graphite at the beginning of the cells than at the end. These cells are quite large, and can even be seen with the naked eye. The boundaries are quite definite, consisting of very fine pearlite, and there is a distinct lack of any kind of

graphite in these regions. Several of these cells are so large that zone transitions lie across them. Upon higher magnification, there does not appear to be any distinct differences in the structure between the two regions solidified in high or low gravity.

There appears to also be dendrites present in the sample, but they are not very distinguishable.

A eutectic cell count was done along the length of the sample, and the results are given below.

Gravity Level	Eutectic Cells /mm^2
1L	---
1H	---
2L	---
2H	2.59
3L	2.59
3H	4.61
4L	2.59
4H	4.61
5L	4.61
5H	2.59
6L	10.38
6H	2.59
7L	10.38
7H	2.59
8L	4.61
8H	4.61
9L	2.59

5.4 Sample 84-F-4 (pure Fe-C-Si-P alloy), R=2.05 mm/min.

The interface on this sample is very evident, and is similar in nature to that seen on other samples. There is a very thin band of fine pearlite, and a eutectic cell structure immediately follows which continues to the end of the sample. Also, well defined dendrites are present throughout the sample.

As in the other sample (84-F-4, R=0.8 mm/min), the leading edges of the eutectic cells seem to have more flake graphite present. Throughout the sample, primary graphite formations can be seen, both within the cells and in the intercellular regions. As in the other sample also, these cells are quite large and well defined, and the intercellular regions consist of fine pearlite, with a distinct lack of eutectic graphite.

A eutectic cell count was done along the length of the sample, the results are shown below, and are shown graphically in Figure 3.

Gravity Level	Eutectic Cells $/mm^2$
1L	4.61
1H	4.61
2L	4.61
2H	2.59
3L	4.61
3H	4.61
4L	7.21
4H	4.61
5L	4.61
5H	4.61
6L	2.59
6H	7.21
7L	4.61
7H	7.21

5.5   Sample 84-F-11 (pure Fe-C-Si-P alloy), R=2.02 mm/min.

The first low-g, first high-g and second low-g zones are virtually identical on this sample. The structure consists of very fine randomly oriented flake graphite surrounded by fine pearlite. An occasional primary graphite formation or area of lighter pearlite is also observed.

At the transition from second low-g to second high-g, the structure begins to deteriorate into more of a cellular structure. More primary graphite is present and all flake graphite is still randomly oriented.

At the third low-g-third-high-g transition, this is even more evident and the structure is about 50% fine pearlite and 50% austenite (cell boundaries).

By the transition from fourth low-g to fourth high-g, the structure is now definitely cellular in nature and large graphite formations are present. It is difficult to say if they are primary or eutectic because they are not highly oriented in any direction. Regardless, they are much larger than the finer graphite seen throughout the sample. From here on, the sample appears to be split longitudinally with respect to structure. While still cellular, one side exhibits much larger eutectic cells than the other. On both sides, the cell size appears to grow as solidification proceeds.

As mentioned earlier, graphite formations are present to the end of the sample. The number, size and thickness of these graphite formations increases toward the end of the sample, probably due to flotation. A eutectic cell count was done along the length of the sample beginning in the second high-g zone (appearance of first cells). The results are shown below, and graphically in Figure 4.

Gravity Level	Eutectic Cells /mm^2
2H	11.81
3L	6.64
3H	7.79
4L	11.81
4H	11.81
5L	9.04
5H	9.04
6L	7.79
6H	5.58

5.6 Sample 84-F-6 (pure Fe-C-Si-P alloy), R=4.08 mm/min.

The first low-g zone seems to be divided into two regions. The first half of this zone is cellular in nature with randomly oriented flake graphite surrounded by austenite and very fine pearlite throughout the matrix. The second half of this zone consists of large eutectic graphite flakes which are directionally oriented in the solidification direction except at the walls where they grow inward, perpendicular to the solidification direction. These flakes are generally surrounded by a thin layer of austenite but the matrix is composed primarily of very fine pearlite.

The transition from first low-g to first high-g, shown in Figure 5a, introduces a structure which is similar to that seen in the first half of the first low-g zone, but there are also eutectic cells present here, and throughout the rest of the sample. These cells appear to get larger along the length of the sample, but are not well defined enough for good quantitative analysis. Dendritic growth also begins at this transition and dendrites are present to the end of the sample. These are pearlitic dendrites and some grow along the entire remaining length of the sample.

Throughout the sample, there are also some primary graphite formations present. Some of these are spherical but others, like the one shown in Figure 5b, have a star-like or exploded shape.

Dendrite arm spacing was measured along the length of the first high-g and second low-g zones, and the results are shown below and graphically in Figure 6.

Location in Sample	Distance from Primary Melt Interface mm	Dendrite Arm Spacing mm
1st Hi-g (1)	2.38	0.057
"	2.90	0.057
"	3.42	0.040
"	3.94	0.036
"	4.46	0.040
"	4.98	0.033
2nd Lo-g	5.50	0.033
"	6.02	0.040
"	6.54	N/A
"	7.06	0.029

(1) All measurements were made on the same dendrite.

5.7 Sample 84-F-6 (pure Fe-C-Si-P alloy), R=4.85 mm/min.

This sample is similar to others in that it consists of a eutectic cell structure as seen in other high phosphorus samples. Throughout the sample, these cells are somewhat smaller at the very edge of the sample, due to a higher cooling rate. They also appear to be smaller in the center of the sample.

Dendrites are present throughout the sample, and in the first low-g zone, grow at more of an angle to the interface than in the rest of the sample. This could be due to irregularities in the furnace translation at the start of solidification.

There is a concentration of flake graphite in the first high-g zone, and they grow larger and fewer in the second low-g zone. Some of these larger formations act as nuclei for dendritic growth.

Dendrite concentration is higher on the edges of the samples than in the middle. The longer dendrites start growing in the second high-g zone and most of these grow through at least one low-g-high-g transition.

5.8 Sample 84-F-3 (pure Fe-C alloy), R=5.17 mm/min.

The interface on this sample is marked by a small band of pearlite globules and is followed by a very fine lamellar pearlite/carbide structure. This structure is present throughout the sample and there are areas where these lamellae appear very oriented in the solidification direction and also where they appear oriented almost parallel to the solidification front.

A band of pearlite-carbide eutectic with much greater interlamellar spacing than the rest of the directionally solidified eutectic was located approximately three-fourths of the way through the first high-g zone (Figure 7a). It is quite short and obviously oriented in the solidification direction.

There is another remarkable structural discontinuity located in the center of the fourth high-g zone. It is made of pearlite globules and carbides, as shown in Figure 7b.

The interlamellar spacing was measured along the entire length of the sample. The results are shown below:

Zone	Distance from Interface mm	Interlamellar Spacing mm
1st Lo-g	0.2	0.00756
	1.2	0.00495
	2.3	0.00551
1st Hi-g	2.5	0.00568
	3.5	0.00685
	4.5	0.00629
	5.5	0.00571
	6.4	0.00602
2nd Lo-g	6.6	0.00528
	7.6	0.00496
	8.5	0.00399
2nd Hi-g	8.7	0.00411
	9.5	0.00431
	10.6	0.00524
	11.7	0.00488
	12.4	0.00504
3rd Lo-g	12.6	0.00498
	13.5	0.00438
	14.4	0.00430
3rd Hi-g	14.6	0.00377
	15.8	0.00387
	17.0	0.00365
	18.2	0.00354
4th Lo-g	18.5	0.00373
	19.4	0.00379
	20.3	0.00433
4th Hi-g	20.6	0.00355
	22.4	0.00365
	24.4	0.00382

5.9 Sample 84-F-9 (pure Fe-C-Si alloy), R=4.89 mm/min.

Directional solidification started in a low-g zone. Immediately after the melt interface the structure exhibits some flake graphite, part of it being primary graphite. This structure ends in the middle of the first low-g zone, and is followed by a much finer irregular and flake graphite structure, as shown in Figure 8.

The transition from first low-g to first high-g shows a decrease in graphite size. Also, whereas there are no dendrites in the first low-g zone, dendritic growth begins in the first high-g zone and dendrites are present in the rest of the sample (Figure 9). The transition from first high-g to second low-g does not show much change in the structure. However, along the entire length of the sample, inclusions at the wall or the presence of the wall itself acted as nuclei for primary graphite formation. These would grow out from the wall, usually at slight angles from the interface (less than 30 degrees) and several times seemed to grow forward in the solidification direction. Following the transition from second low-g to second high-g, coarsening of the graphite can be seen. A band of primary graphite was evident at the end of the third low-g zone, extending a little in the third high-g zone.

Although it cannot be seen on Figure 9, primary graphite grows along the wall of the crucible well into the third high-g zone. It should be noted that in the region where primary graphite is very large (from one third of the way into the second high-g zone all the way to the end of the third low-g zone), dendritic growth is much less noticeable, and any dendrites present are quite small. However, the transition from the third high-g to third low-g zones marks the beginning of long dendrites, some of which grow to the end of the sample (fourth high-g zone). Almost all of these dendrites grow virtually perpendicularly to the interface, in the direction of solidification.

Coarsening of the graphite was also noted toward the end of the sample, in the fourth high-g zone.

Dendrite arm spacing was measured on dendrites growing across some transitions (see Discussion).

5.10 Sample 84-F 3 (pure SG iron), R=4.97 mm/min.

The nodules in the first low-g zone are quite small and the nodule count is high. This changes however, in the first high-g zone as the nodules become larger and the nodule count decreases (Figure 10).

No significant changes occur until the middle of the second low-g zone, where carbides and dendrites begin to form in the center of the sample, and by the end of the second low-g zone, extend all the way to both walls. However, along the length of the sample there is a thin band of very small nodules, with no carbides along the walls, on both sides of the sample. All dendrites grow in a direction close to that of the heat flow.

At about the middle of the second and third high-g zones, a higher nodule count can be observed.

It is difficult to interpret the structure starting with the second high-g zone because of the presence of a rather complex structure consisting of graphite nodules, carbides and pearlite.

Measurements of nodule counts were made in the first high-g and second low-g zones in an attempt to determine if a relationship exists between gravity and nodule count. The results are shown below and graphically in Figure 13.

Distance from Melt Interface mm	Gravity Level	Nodule Count nodules/mm^2
3.2	1st High-g	158.0
3.8		159.4
4.4		125.4
5.0		113.6
5.9		112.3
7.1	2nd Low-g	134.5
7.8		129.3
8.6		135.8

The first low-g zone was not considered because of irregularities in the melt interface and no zones were considered after the second low-g zone because of the presence of carbides in the sample after the second low-g zone.

6. DISCUSSION

6.1 Sample P-2, R=5.16 mm/min.

The solidification behavior of the pure Fe-C-Si iron (sample P-2) during KC-135 flights seems to be very similar in nature with that of the high-phosphorus commercial composition iron (sample C-41c) on which we have reported earlier. Indeed, a band of highly oriented flake graphite was found to occur in the middle of the first high-g zone, following a low-g zone. This is considered to be a transition from irregular (or cellular solidification) to cellular (or planar solidification). In any event this can also be characterized as a coarsening of the structure. Also evident are irregular graphite formations, the formation of which will require more study.

6.2 Sample P-2, R=2.00 mm/min.

This sample also exhibits a phenomenon which has been observed in other samples. At the end of the seventh high-g zone, a band of large, randomly oriented flake graphite is present across the width of the sample. This is probably due to the entrapment by the interface of floating graphite formations. Irregular graphite formations present in this sample also warrant more study.

6.3 Samples 84-F-4, R=0.8 and 2.05 mm/min.

Both of these samples exhibit well defined interfaces of dense pearlite which differ only in thickness. In both samples, this is immediately followed by formation of eutectic cells. At the slower growth rate, the size of these cells remains somewhat larger than those in the other sample.

6.4 Sample 84-F-11, R=2.02 mm/min.

As in the previous high phosphorus samples, fine pearlite is the main structural feature in the early stages of solidification. However, as in the other samples also, this deteriorates into a cellular structure. The results of a eutectic cell count are shown in Figure 4 and it can be seen that there is a slight coarsening of the cell size as solidification proceeds in the sample.

6.5 Samples 84-F-6, R=4.08 and 4.85 mm/min.

At R=4.08 mm/min, there is an interesting anomaly at the beginning of the sample. The first half of the first low-g zone is cellular, but the second half is marked by directionally oriented eutectic flake graphite. This has been seen in other samples (P-2, R=5.16 mm/min), and can be attributed to the nature of the interface changing from cellular to planar.

As opposed to the other samples (%P=0.10), this sample (%P=0.25) has definite dendritic growth within the sample, indicative of the influence of phosphorus, which is to generate a more irregular structure. As shown in Figure 6, the arm spacing of these dendrites

appears to be refined during the solidification process. There does not appear to be a correlation between gravity level and arm spacing.

6.6 Sample 84-F-3, R=5.17 mm/min.

It is interesting to note that a significant structural discontinuity occurred in the middle of the first and at the beginning of the fourth high-g zones. This phenomenon is similar in nature with the coarser graphite observed in previous gray iron samples in some of the high-g zones.

The first discontinuity, shown in Figure 7a, maintains a rather high degree of orientation, as opposed to the second discontinuity, shown in Figure 7b, where the pearlite is randomly disributed as spheroids. This could be rationalized in terms of higher constitutional supercooling in the last part of the sample to solidify, because of higher solute content. It seems reasonable to assume that the first discontinuity has a cellular structure, while the second one has a dendritic or irregular type structure.

The variation of the interlamellar spacing of the eutectic along the length of Sample 84-F-3, is shown in Figure 11. In general, it can be stated that the interlamellar spacing decreases sharply along the low-g zones, while increasing toward the middle of the high-g zones. Overall the spacing is decreasing along the length of the sample. In other words, the substructure of the eutectic is refined in the low-g zones.

6.7 Sample 84-F-9, R=4.89 mm/min.

Several graphite lamellae, apparently nucleating at or near the wall, have been observed growing perpendicular to the wall, or in the direction of solidification (that is, against the direction of the heat flow), which suggests that the crystallographic growth direction is more important in the growth process of primary graphite than the direction of the heat flow.

The variation of the secondary arm spacing along several dendrites throughout low-g-high-g transitions is shown in Figure 12. It can be seen that the dendrite arm spacing increases at high-g-low-g transitions, and decreases at low-g-high-g transitions. In other words, a coarsening of the structure occurs when the gravity level decreases.

6.8 Sample 84-F-8, R=4.97 mm/min.

The graph showing the variation of the nodule count along two zones of the sample in Figure 13 can be interpreted again in terms of the coarsening of the structure coinciding with the decrease in the gravity level, as evident in the middle of the first high-g zone. This type of behavior has also been observed in commercial iron sample C-51, shown in Figure 14 (1). However, this assertion is not supported by the data in the second low-g zone. But this could be explained by solidification catching up with flotation in the low-g zone. As long as solidification proceeds in high-g, calculations show that the flotation rate was much higher than the solidification rate. Indeed, the growth rate for this sample was 4.97 mm/min, while the flotation rate (calculated using Stokes' Law) ranged from 23.64 mm/min at the beginning of the first high-g zone to 42.06 mm/min at the end of the first high-g zone.

7. CONTROL SAMPLES

All control samples were processed so as to very accurately reproduce solidification conditions on board the KC-135 aircraft. For example, the first sample melted each day on the aircraft had a longer holding time at the melt temperature. This extra time was measured and the control sample was also held at temperature longer before translation was begun. Of course, melt temperatures and growth rates are the same as those used on the aircraft for a particular sample within experimental error and aircraft limitations.

7.1 Sample P-2, R=4.79 mm/min.

The interface is quite clear as it is marked by a band of eutectic graphite which is oriented in the direction of solidification. Another band of unoriented primary graphite seems to extend from the interface between metal that melted and ran between the sample and crucible and the sample itself. This growth is on both sides of the sample and continues further into the sample.

Just past the interface, the structure looks like a typical hypereutectic alloy, with primary graphite and fine flake graphite randomly dispersed throughout the sample. None of this graphite appears to be oriented. There are a couple of areas of primary graphite growth further in the sample that are also not oriented. Dendritic growth is also present and the dendrites do appear to be oriented in the direction of solidification. There is a concentration of primary graphite at the end of the sample that is unoriented. Since graphite being rejected in front of the interface would not or could not grow backwards and because of the presence of gravity, it is assumed that graphite flotation is the cause of this segregation at the end of the sample.

7.2 Sample 84-F-6, R=5.06 mm/min.

The interface is clearly marked by a thin band of large directional eutectic graphite flakes surrounded usually by ferrite but also by very fine pearlite.

The rest of the sample appears to be randomly oriented thick eutectic graphite flakes surrounded by ferrite but is interdispersed with very fine pearlite. Randomly dispersed throughout the sample are what appear to be pearlite nodules which are quite well defined.

Pearlitic dendrites are also present throughout the sample. These dendrites are highly oriented in the solidification direction. There is a large concentration of graphite formations at the end of the sample. They are quite irregular in shape and indicate graphite flotation.

There is a eutectic cell structure present due to the high phosphorus content, but it is not easily detected along the entire length of the sample. A eutectic cell count was done along the length of the sample, and the results are given below and shown graphically in Figure 15.

Average Distance from Melt Interface mm	Eutectic Cells /mm^2
2	7.79
4	6.10
6	4.61
8	4.61
10	3.33
12	4.61
14	6.10
16	2.95
18	4.61

7.3 Sample 84-F-9, R=-5.00 mm/min.

At low magnification, the interface is not very evident, but is
very much so at higher magnification (400x). There is a very thin band
of austenite surrounding large eutectic graphite formations that are
highly oriented in the direction of solidification at the interface.
After this band, the structure then assumes a typical hypereutectic
structure, with both fine eutectic flakes and larger primary graphite
dispersed throughout the austenite matrix.

Dendrites are present throughout the sample and become more
oriented in the direction of solidification as the solidification front
advances through the sample. About one-third of the way into the
sample, larger primary graphite formations begin appearing and their
concentration increases to the end of the sample, obviously a result of
graphite flotation. Primary graphite is also noted nucleating at both
crucible walls and this graphite grows both in and against the
solidification direction.

7.4 Sample 84-F-3, R=4.69 mm/min.

At higher magnification (200x), the interface is very evident as
fine unoriented lamellae changes to a highly oriented lamellar
structure. At the interface, there is a small band of pearlite globules
present, but they are not present anywhere else in the sample.

There are several austenite dendrites present in the sample.

An interesting feature is shown in Figure 16; cells can be seen
growing in the direction of solidification, but also other cells
intersect one another, suggesting there is a preferred local growth
direction (crystallographic direction).

7.5 Sample 84-F-8, R=5.19 mm/min.

This sample is similar to the flight sample in that it has an area at the beginning of the sample that is free of carbides. It is a spheroidal graphite structure from the interface to a distance of about 4.5 mm. The formation of carbides begins in the center of the sample and as solidification proceeds until, almost to the end of the sample, the carbides extend to both crucible walls. These spheroids and carbides appear to get larger along the length of the sample.

Ledeburite and pearlitic dendrites are also present in this sample. Virtually all of the dendrites and carbides are oriented in the solidification direction. Nodule counts were made on this sample from the interface to the initial formation of carbides, and the results are shown below and graphically in Figure 17.

Distance from Interface mm	Nodule Count nodules/mm^2
0.16	240.12
0.46	109.62
0.82	130.50
1.11	161.82
1.54	125.28
1.84	146.16
2.22	135.72
2.53	182.70
2.91	193.14
3.20	177.48
3.57	109.62
3.87	120.06

8. CONCLUSIONS

A number of experimental conclusions result from the above work, which could be summarized as follows:

o   For a pure Fe-C white iron it was found that the interlamellar spacing in the austenite-carbide eutectic decreases along a low-g zone. The spacing increases toward the middle of high-g zones, and then decreases again toward the end.

o   For a pure Fe-C-Si gray iron it was found that the secondary austenite dendrite arm spacing decreases during the transition from low-g to high-g zones, and, on the contrary, increases at high-g to low-g transitions.

o   For a pure Fe-C-Si spheroidal graphite cast iron sample it was found that the nodule count increases toward the center of the first high-g zone, and is followed by a sharp decrease. This data, at least for these zones, is verified by earlier work.

These experimental conclusions seem to indicate that a coarsening of both the eutectic grain size (eutectic cell count or nodule count) and of the primary (dendritic) structure is associated with a decrease in the level of the gravity, as shown in Figure 18. This interpretation is consistent with experimental data given in the reference on the eutectic cell count of high-phosphorus samples.

Some earlier data on dendrite arm spacing in austenite (1), indicated that the DAS becomes smaller in low-g, which seems to be in contradiction with the results of this report. It should be · ·oned though, that the earlier results are average data for the er' ire zone, while the new data come from measurements at zone boundaries.

o   The eutectic substructure of white iron (interlamellar spacing) is refined during low-g.

REFERENCES

1. Hendrix, J.C., Curreri, P.A., Stefanescu, D.M., "Directional Solidification of Flake and Spheroidal Graphite Cast Iron in Low and Normal Gravity Environment," Space Science Laboratory, Preprint Series, No. 84-128, April 1984.

LIST OF FIGURES

25

KC-135 LOW-G
MANEUVERS

SAMPLE NO.:P-2
COMPOSITION:pure Fe-C-Si
TRANSLATION RATE:5.0mm/min
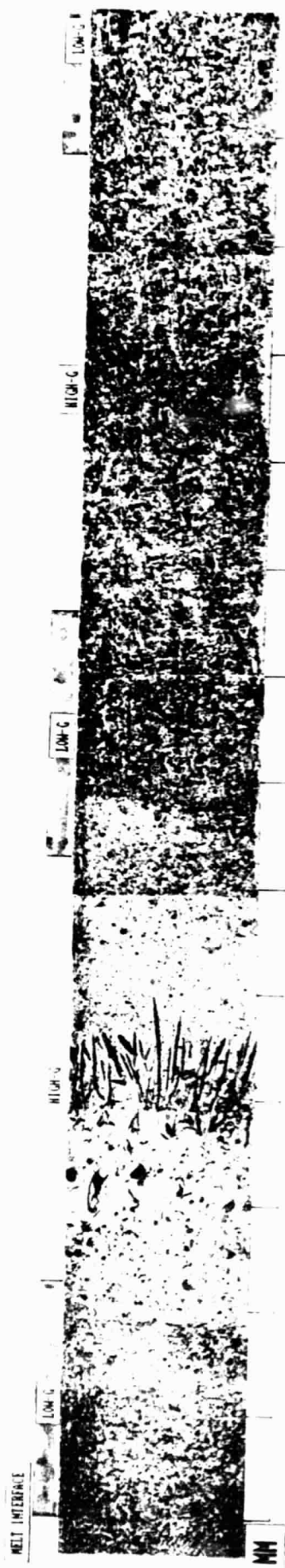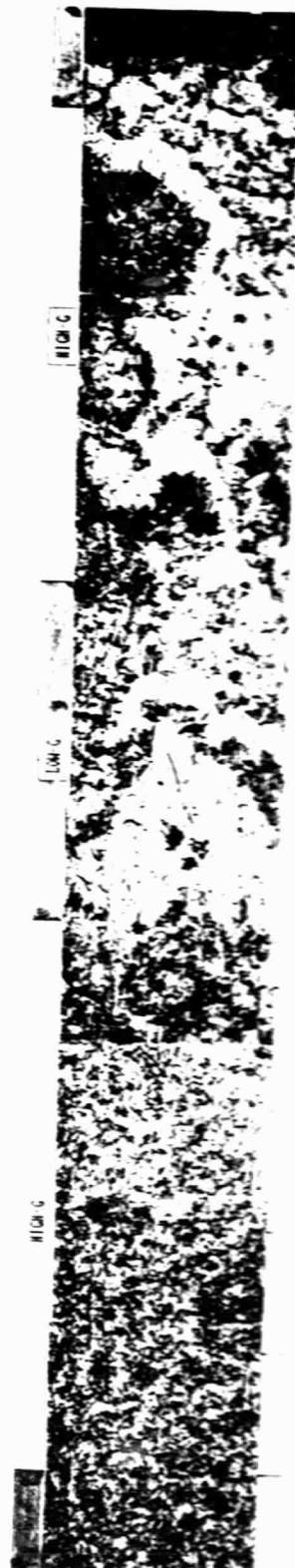
Figure 1

a) Low-G Zone

b) Beginning of High-G Zone

Direction Of Growth --------->

c) Middle of High-G Zone
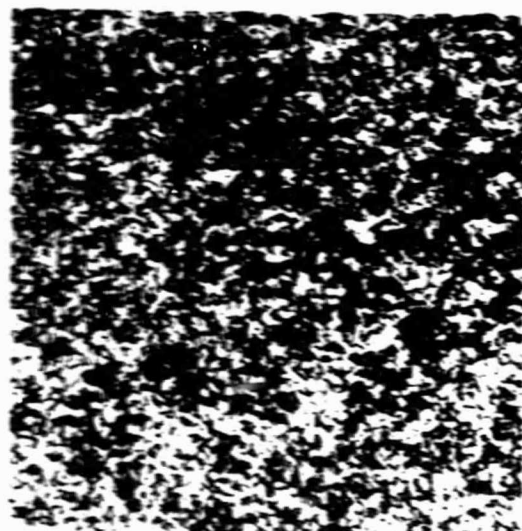
d) End of High-G Zone

Metallographic structures of sample P-2,
from the first low-g and first high-g zones, x100

Figure 1

Fig. 3 – Fe-C-Si-P Sample 84-F-4, R = 2.05 mm/min
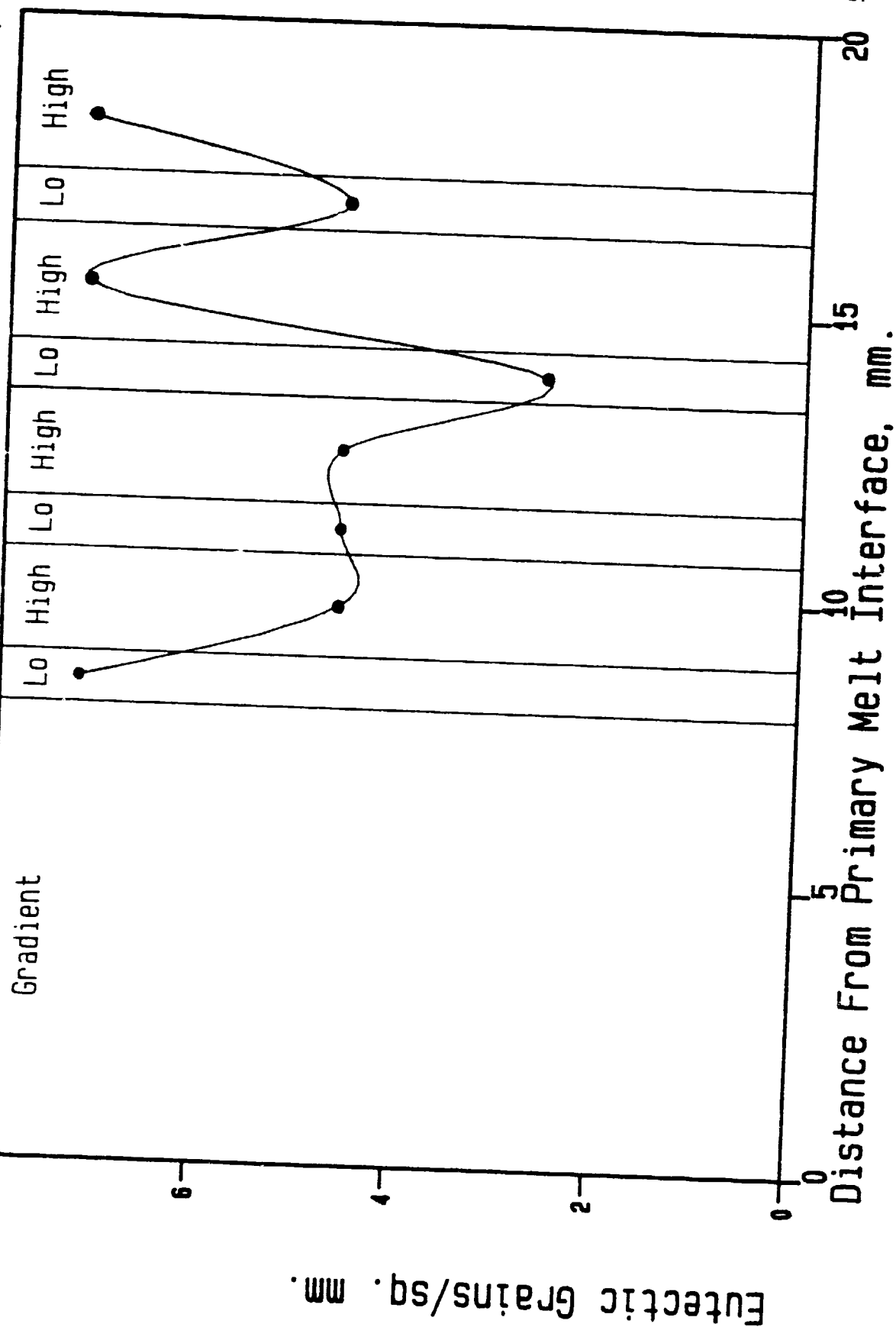
Fig.4 - Fe-C-Si-P Sample 84-F-11, R = 2.02 mm/min.

Eutectic Grains/sq.mm.

Distance From Primary Melt Interface, mm.

Gradient

Low-G   High-G   Low-G   High-G   Low-G
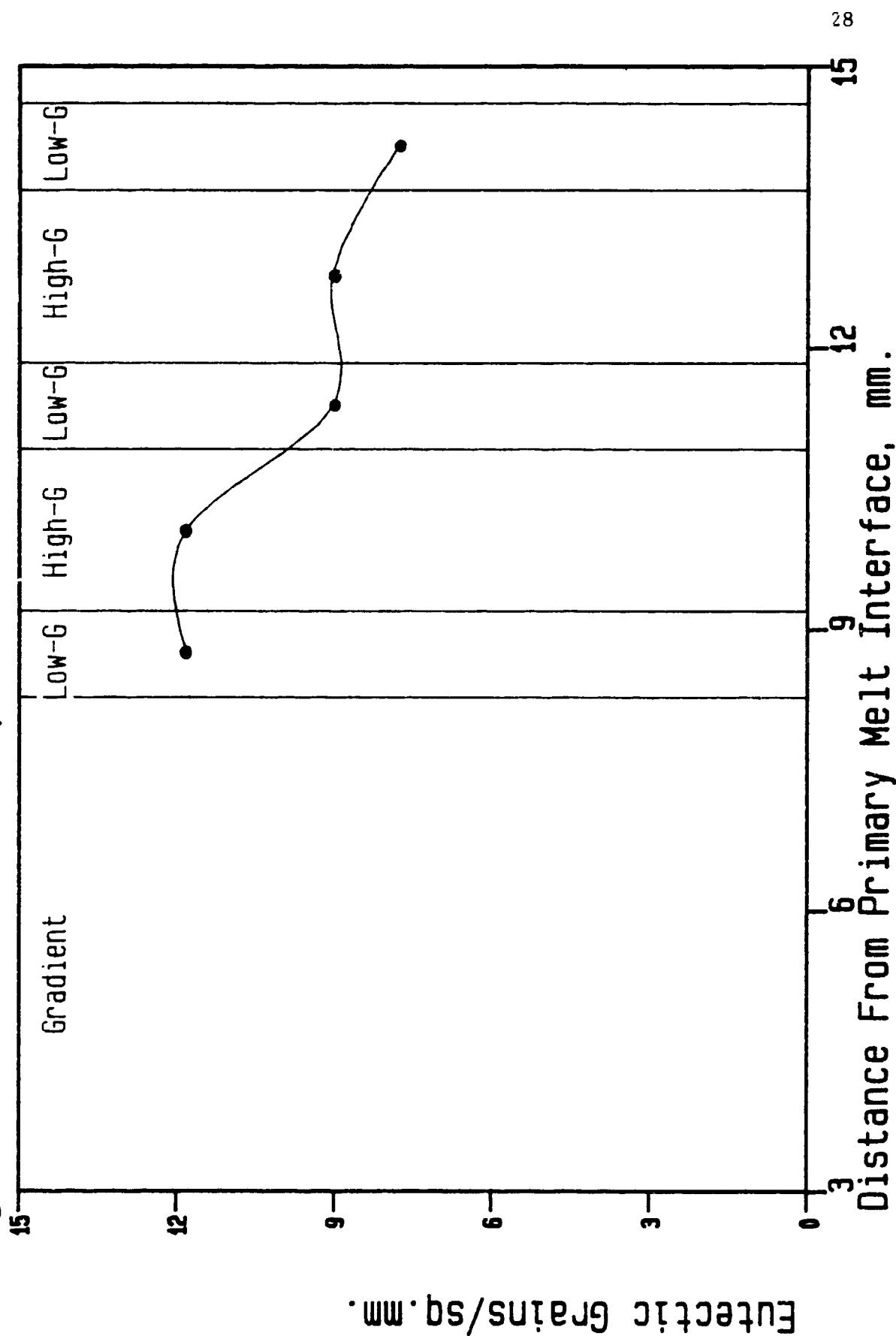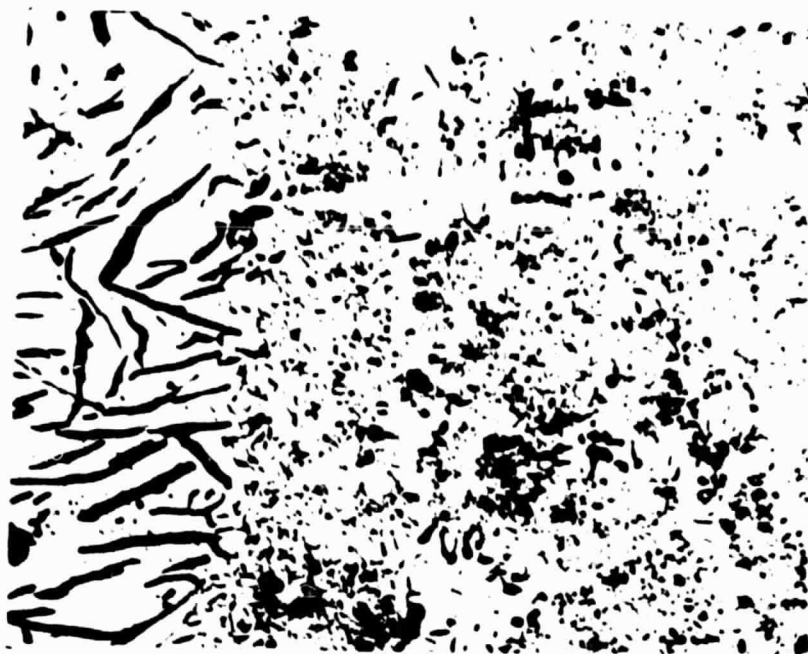
a) 1st Low-g-1st High-g Transition

Direction of Growth ------>
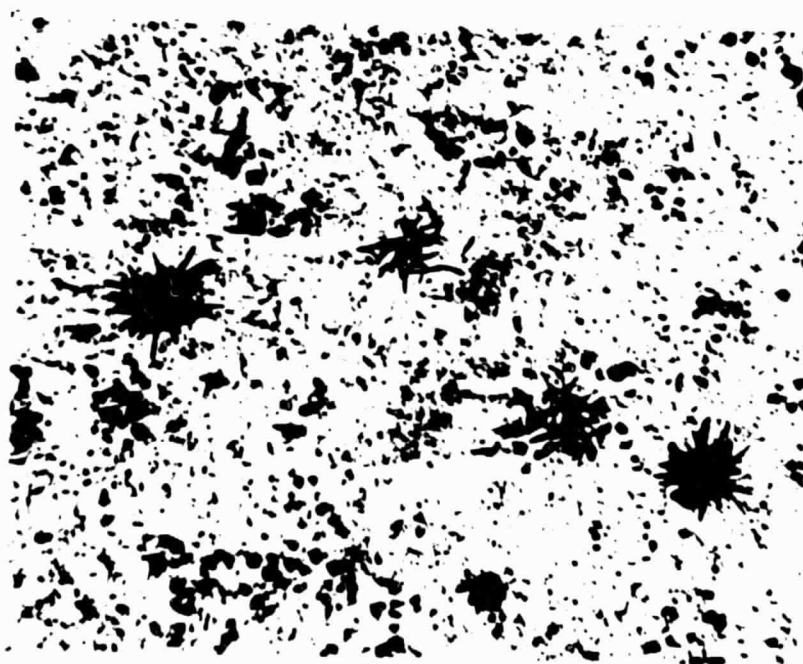
b) Third Low-g

SAMPLE 84-F-6 (Pure Fe-C-Si-P alloy), R=4.08 mm/min.

Metallographic Features, 100x

Figure 5

Fig.6 - Fe-C-Si-P Sample 84-F-6, R = 4.08 mm/min

Secondary Dendrite Arm Spacing, mm.

Distance From Primary Melt Interface, mm.

Low-G

High-G

30
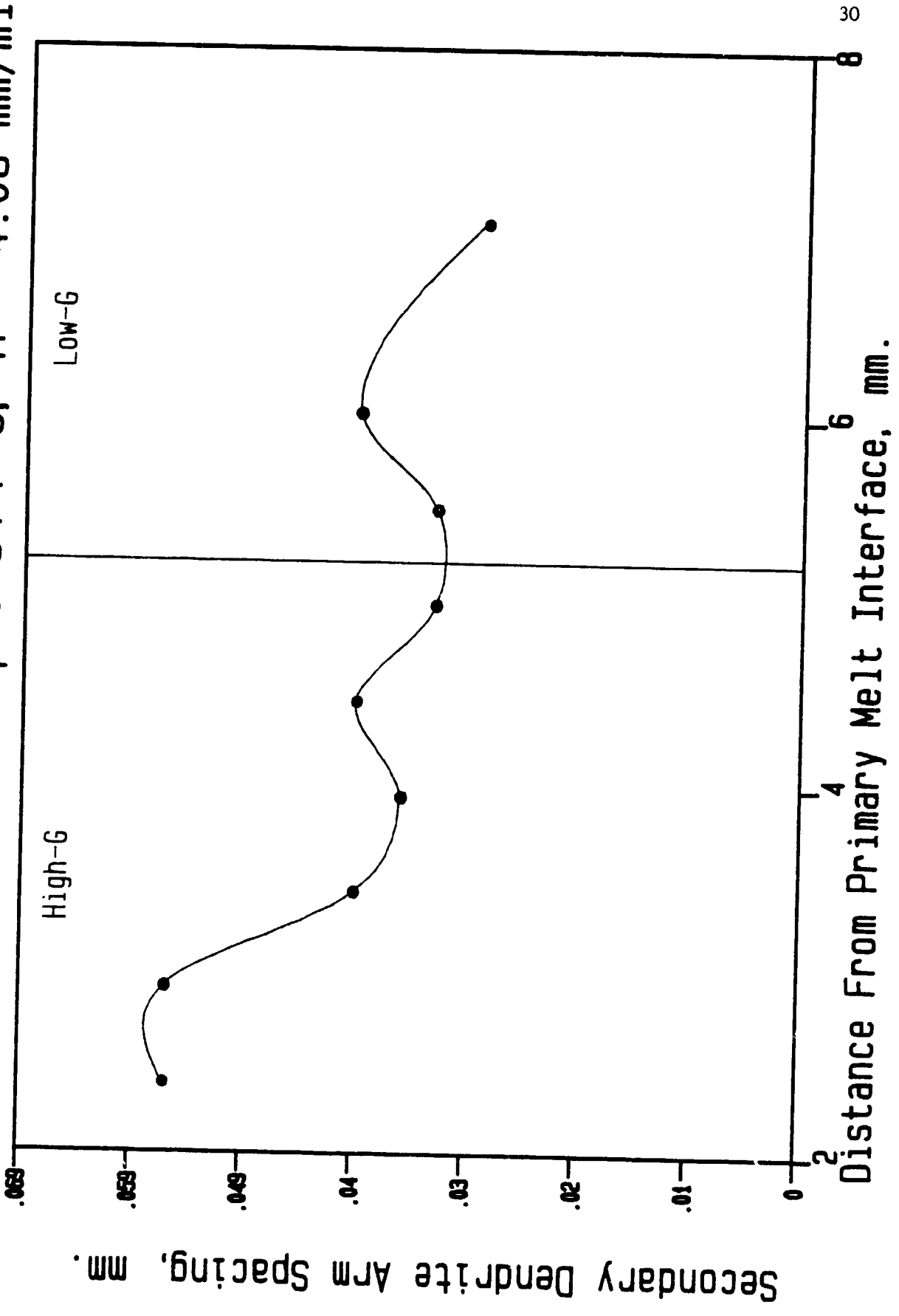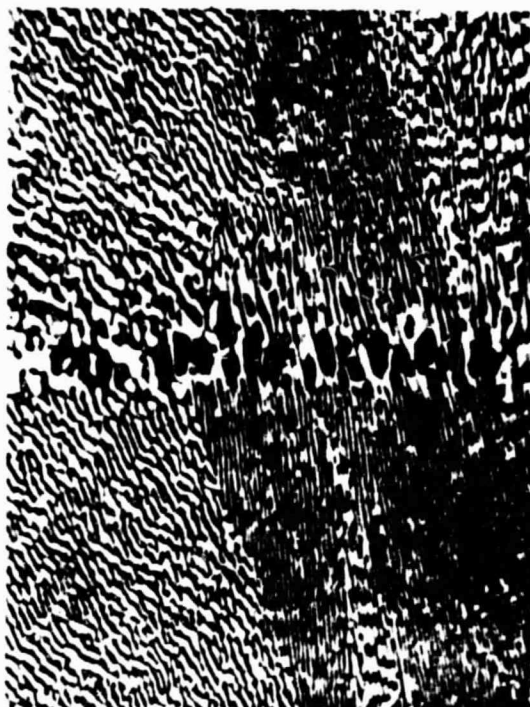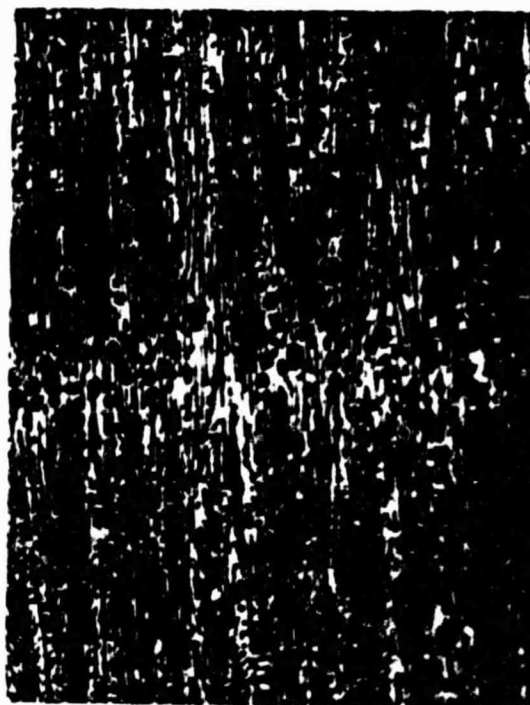
a) First high-g zone   b) Fourth high-g zone

SAMPLE 84-F-3 (Pure Fe-C alloy), R=5.17 mm/min.
Bands in high-g zones, 200x
Solidification direction upward

Figure 7

SAMPLE 84-F-9 (Pure Fe-C-Si alloy), R=4.89 mm/min.
Change in primary graphite shape in first low-g zone, 100x
Solidification direction upward

Figure 8

33

SAMPLE NO.:84-F-9
COMPOSITION:pure Fe-C-Si
TRANSLATION RATE:4.9mm/min

KC-135 LOW-G
MANEUVERS
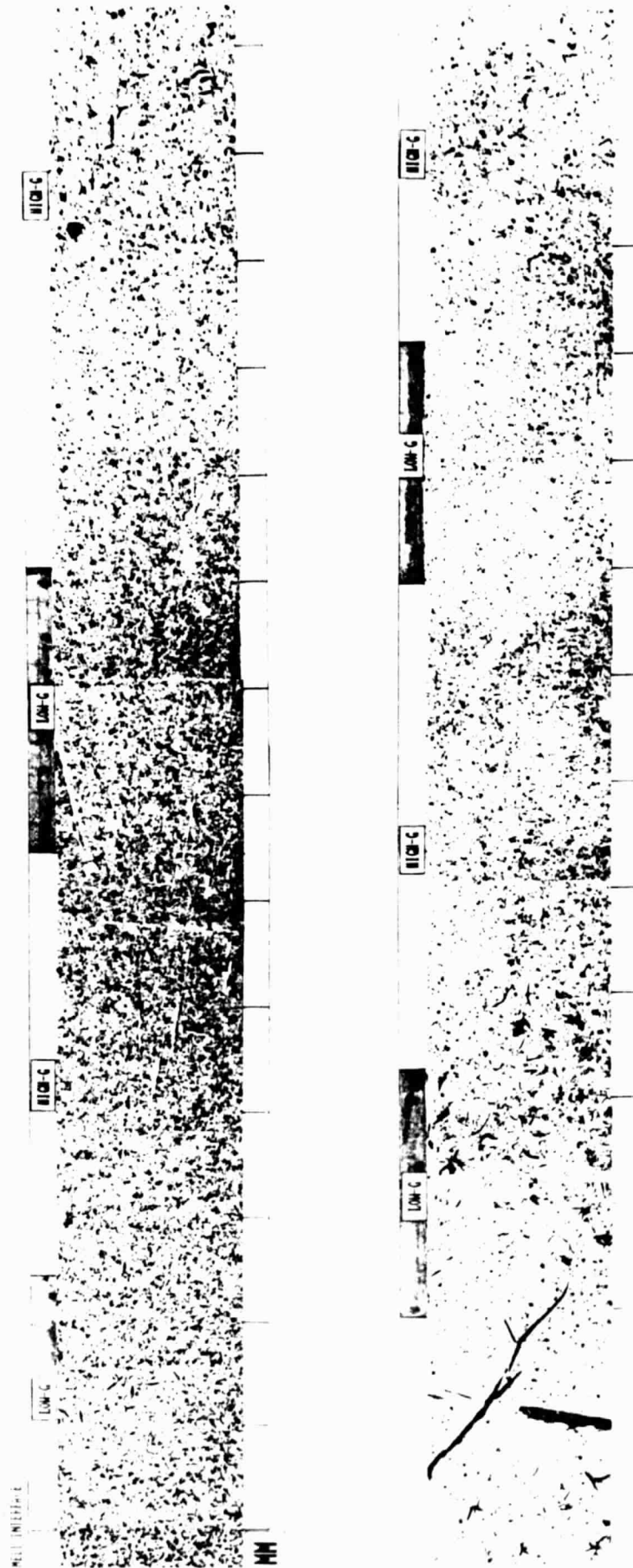
Figure 9

KC-135 LOW-G
MANEUVERS

SAMPLE NO.:84-F-8
COMPOSITION:pureFe-C-Si-Ce
TRANSLATION RATE:5.0mm/min

34
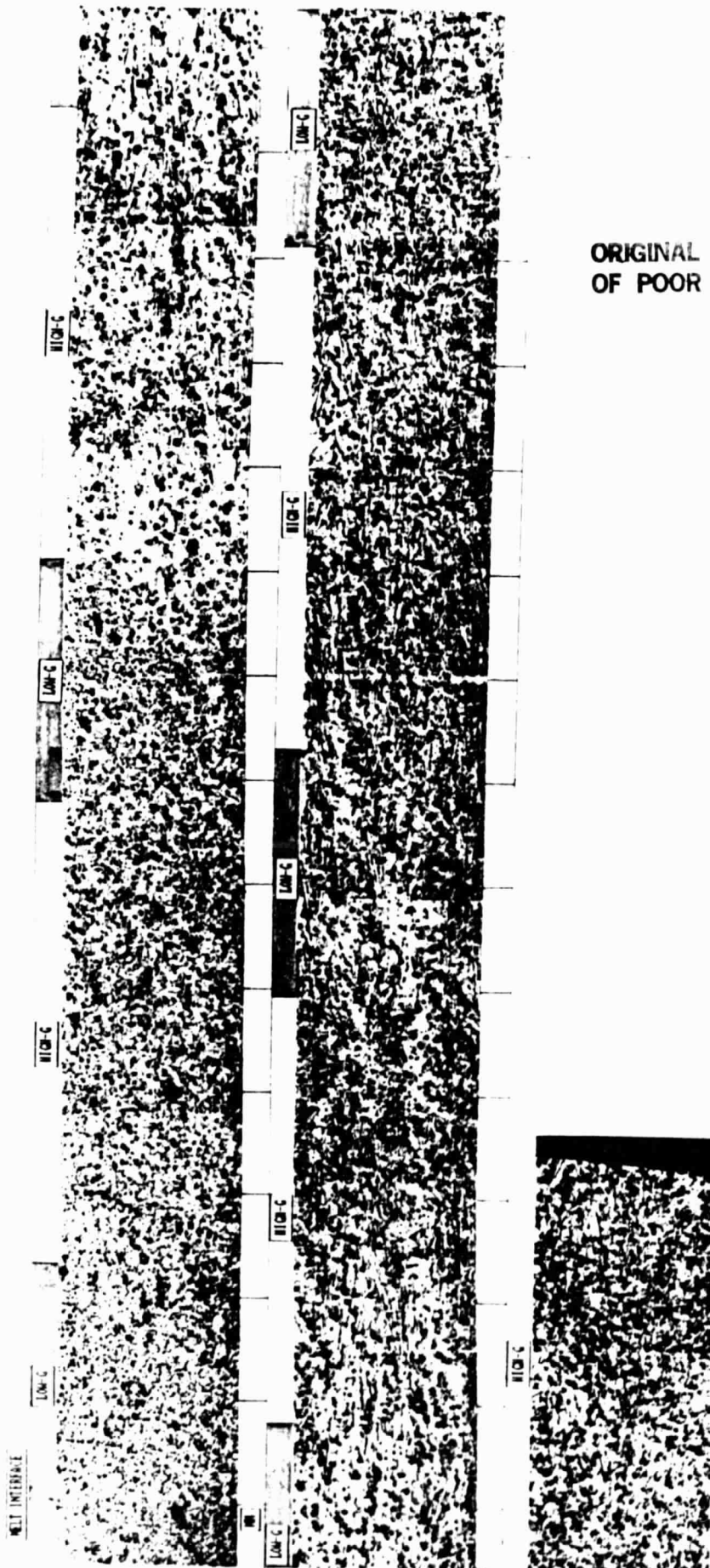
Figure 10

Fig. 11 - Fe-C Sample 84-F-3, R = 5.17 mm/min.

Interlamellar Spacing, mm.

Distance From Primary Melt Interface, mm.

Gradient

Low-G

High-G

Low-G

High-G
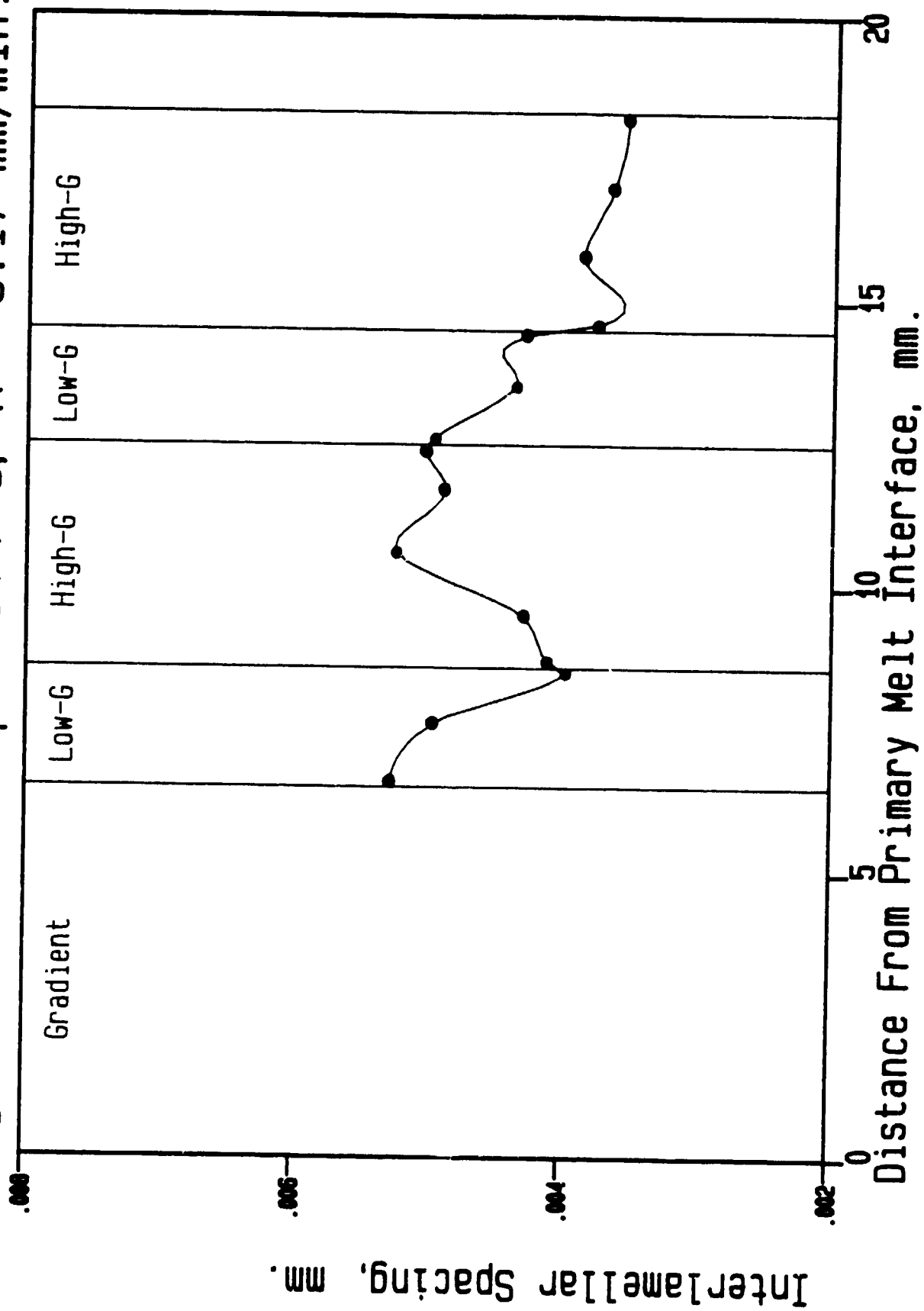
Fig.12 - Fe-C-Si Sample 84-F-9, R = 4.89 mm/min
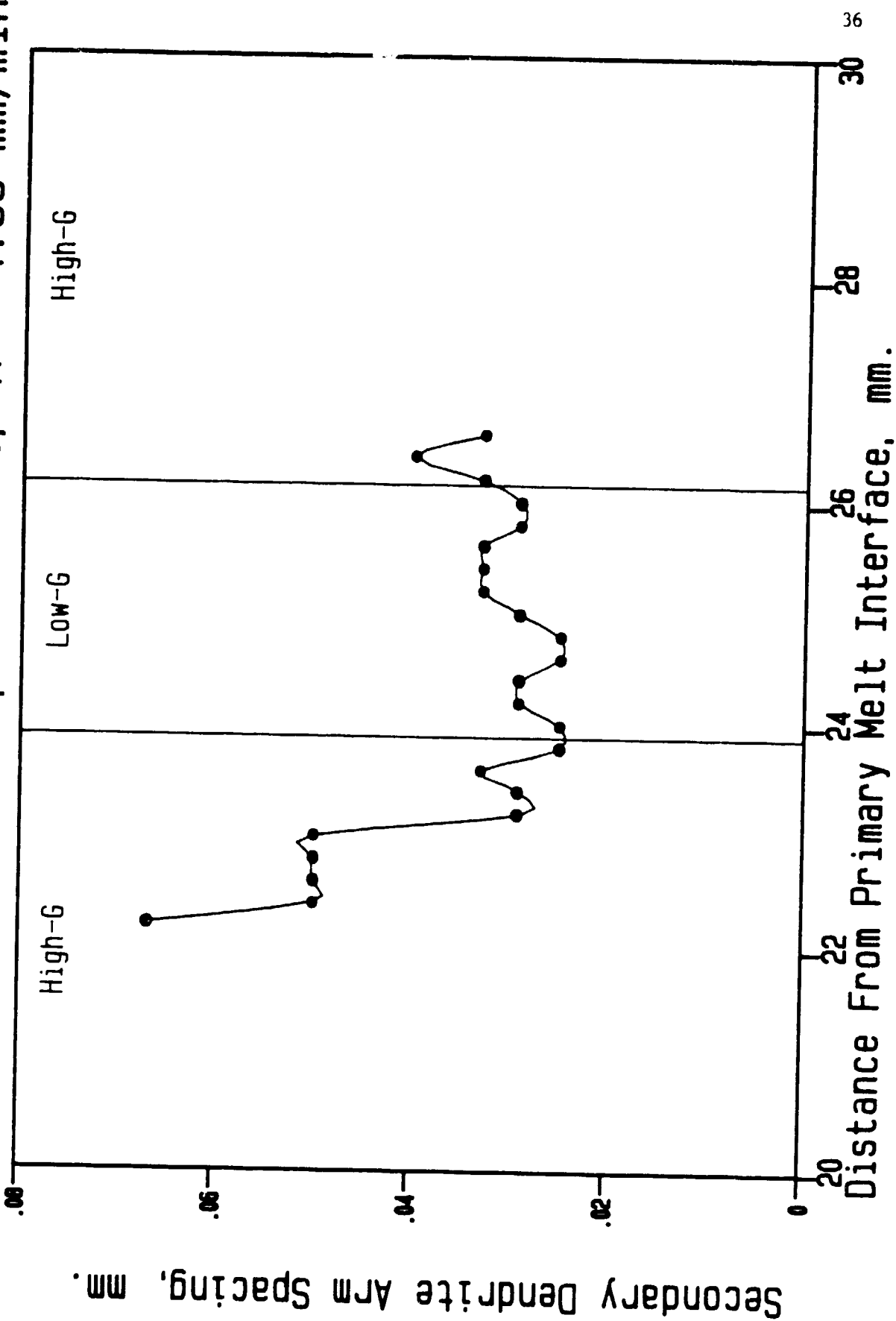
Fig. 13 - Fe-C-Si-Ce Sample 84-F-8, R = 4.97 mm/min
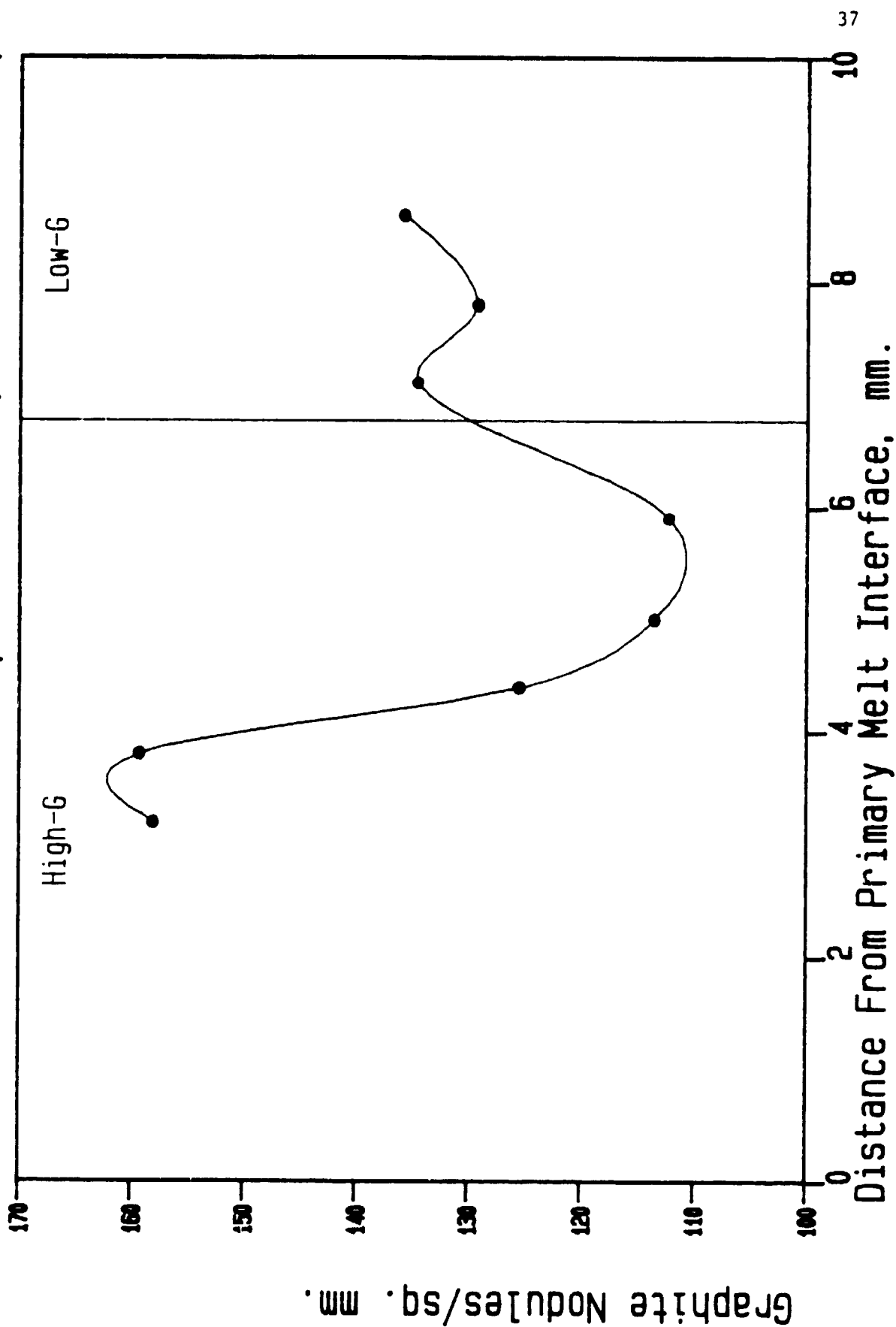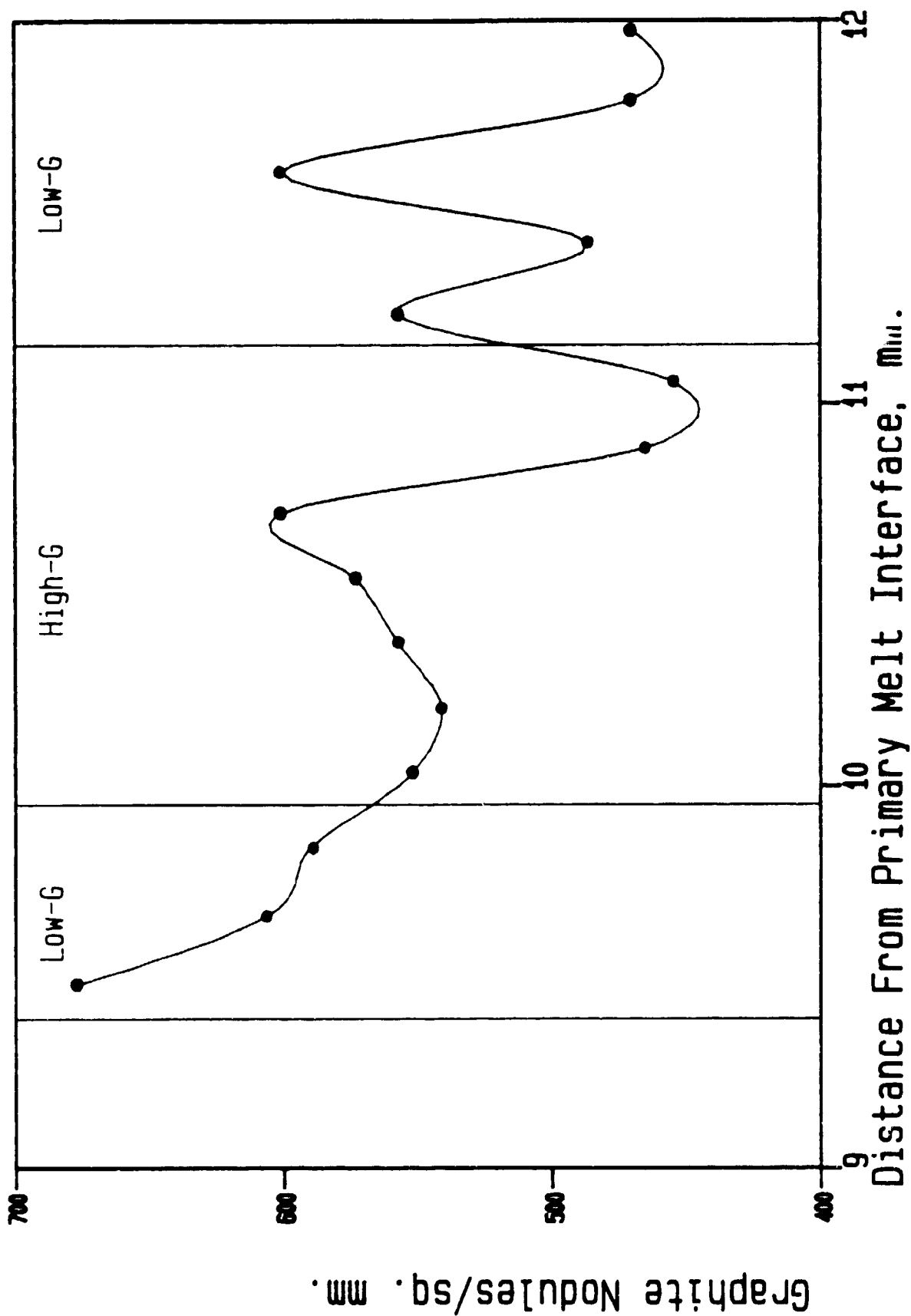
Fig. 14 – Fe-C-Si-Ce Sample C-51, R = 2 mm/min.
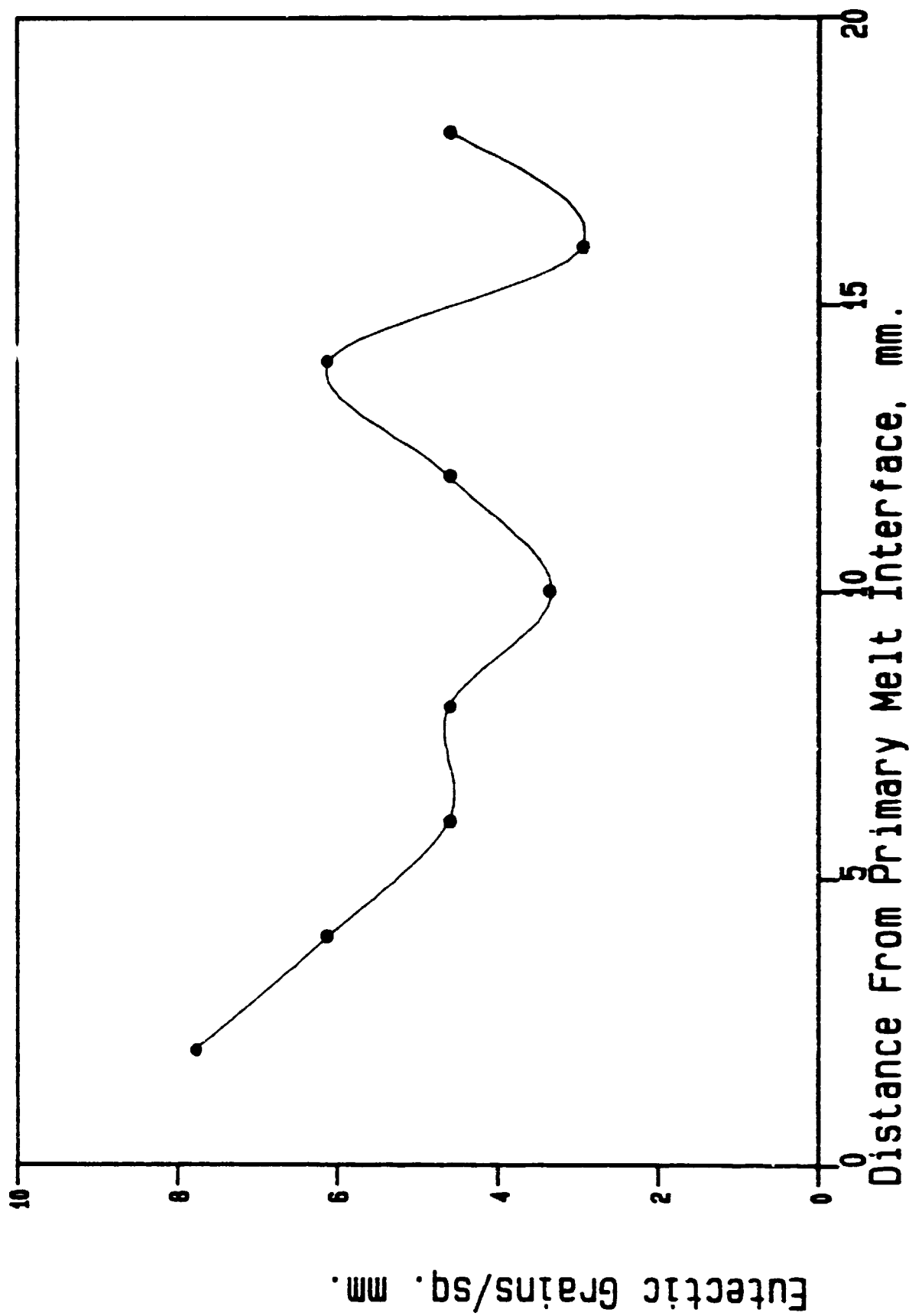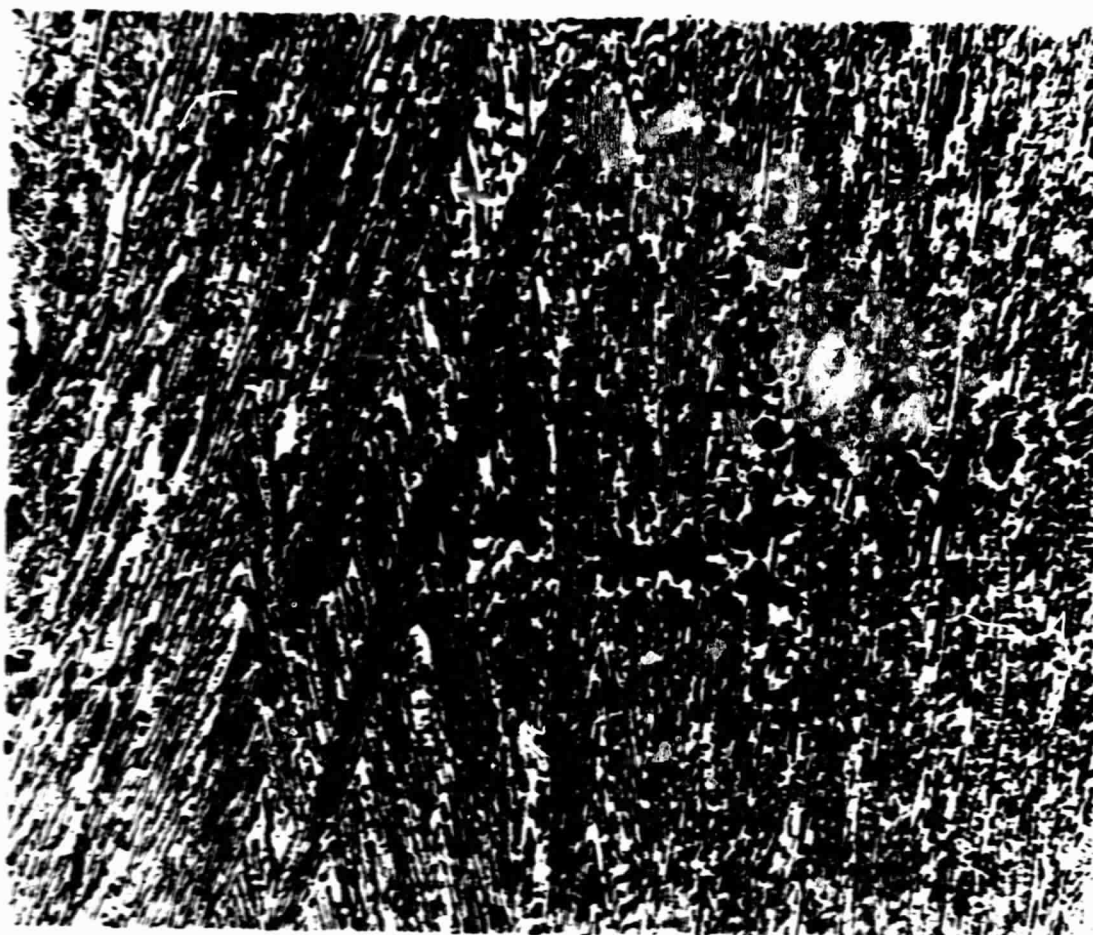
Fig.15 Fe-C-Si-P Control Sample 84-F-6, R=5 mm/min

SAMPLE 84-F-3 Control (Pure Fe-C alloy), R=4.69 mm/min.
Metallographic Structure, 100x
Solidification direction upward

Figure 16

Fig.17 Fe-C-Si-Ce Control Sample 84-F-8, R=5 mm/min
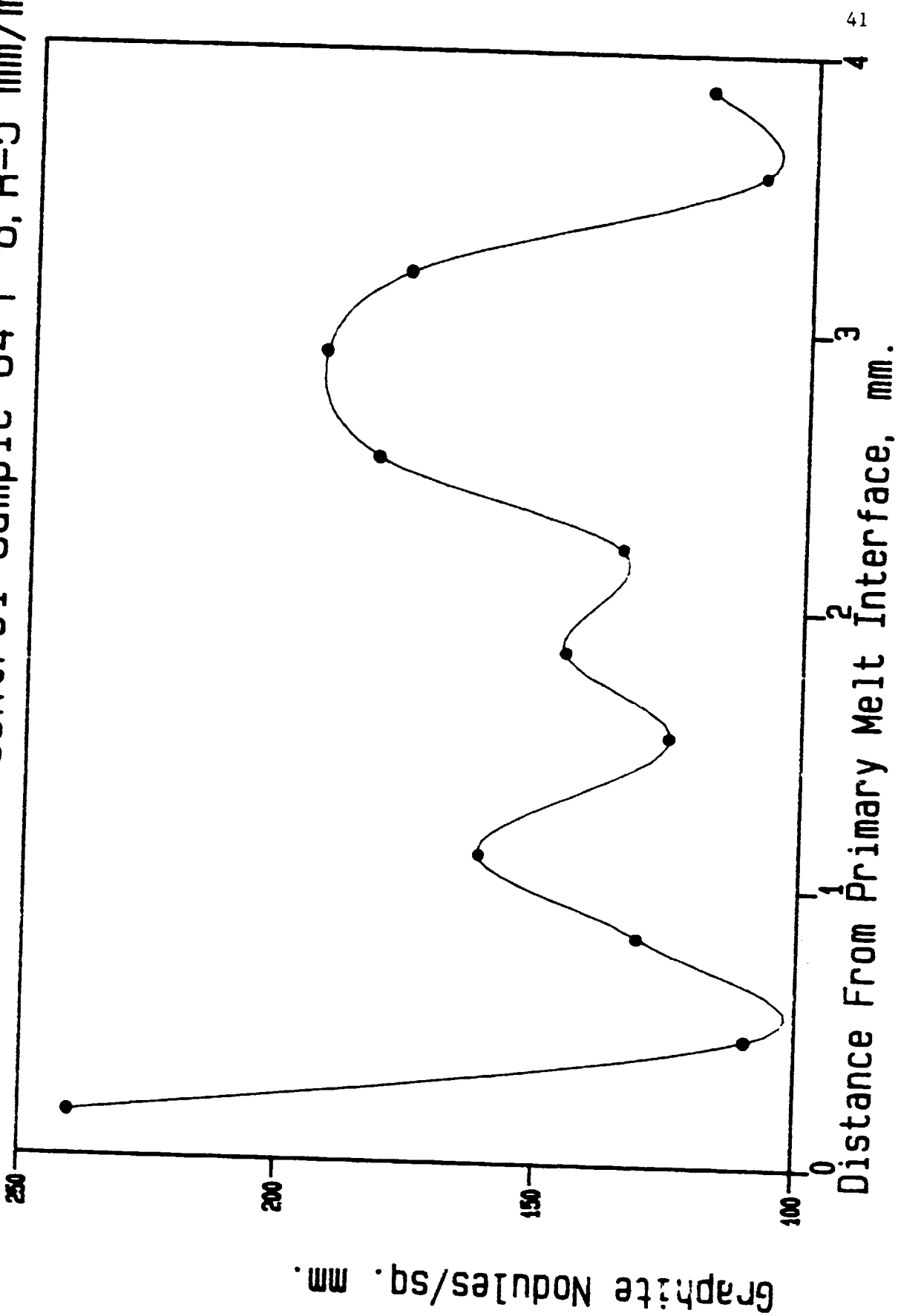
Graphite Nodules/sq. mm.

Distance From Primary Melt Interface, mm.

Fig. 18 - Effect of Gravity Level on Structure

Nodule Count —
Eutectic Grain Count —
Austenite Secondary
Dendrite Arm Spacing —

High-G   Low-G   High-G

Structure Fineness

Gravity Level